

T H E U N I V E R S I T Y O F M I C H I G A N

COLLEGE OF ENGINEERING

Department of Aerospace Engineering
High Altitude Engineering Laboratory

Final Report

THEORETICAL INVESTIGATIONS OF CARBON DIOXIDE RADIATIVE TRANSFER

S. Roland Drayson and Charles Young

ORA Project 07349

under contract with:

U. S. DEPARTMENT OF COMMERCE
WEATHER BUREAU
CONTRACT NO. Cwb-11106
WASHINGTON, D.C.

administered through:

OFFICE OF RESEARCH ADMINISTRATION

ANN ARBOR

August 1966

en 8n

UMR0736

TABLE OF CONTENTS

	Page
LIST OF TABLES	v
LIST OF FIGURES	vii
ABSTRACT	ix
1. INTRODUCTION	1
2. CALCULATION OF ROTATIONAL LINE POSITIONS AND INTENSITIES	2
2.1 Calculation of Rotational Line Positions	2
2.1.1 The carbon dioxide molecule	2
2.1.2 Rotational line positions	7
2.2. Calculation of Rotational Line Intensities	14
3. DIRECT INTEGRATION TECHNIQUES	20
3.1 Introduction	20
3.2 Homogeneous Paths	22
3.3 Slant Paths	24
3.4 Programming Techniques	26
4. HOMOGENEOUS PATH TRANSMISSIVITIES	32
4.1 Calculation of Rotational Line Positions and Intensities	32
4.2 Half-Widths and Line Shapes	36
4.3 Comparison of Calculated and Experimental Transmissivities	37
5. SLANT PATH TRANSMISSIVITY	45
6. CONCLUSIONS	52
ACKNOWLEDGMENTS	53
REFERENCES	54

LIST OF TABLES

Table	Page
2.1 Vibrational energy levels for carbon dioxide in the 12- to 18-micron region	8
2.2 Rotational constants for carbon dioxide in the 12- to 18-micron region	11
4.1 Band intensities used in calculating rotational line intensities	33
4.2 Integrated intensity of the 15-micron CO ₂ bands	34
4.3 Comparison of calculated and experimental equivalent widths	38
5.1 Vertical path transmissivity from 10.0 mb for SIRS	48
5.2 Vertical path transmissivity from 10.0 mb for SIRS	48
5.3 Vertical components of radiance at 10 mb for U. S. Weather Bureau Texas balloon flight	51

LIST OF FIGURES

Figure	Page
2.1. Vibrations of the carbon dioxide molecule and changes in electric moment.	3
4.1. Comparison of calculated absorption with experimental values of Burch et al. (1962).	39
4.2. Comparison of calculated and experimental absorption at 0.39 mm Hg.	43
5.1. Temperature structure for balloon flight.	46
5.2. Comparison of slant path transmission for U. S. Weather Bureau balloon flight, Palestine, Texas, September, 1964.	47

Abstract

Rotational line positions and intensities for the 15-micron carbon dioxide bands have been calculated, taking into account the important carbon dioxide isotopes. This information has been used to calculate transmissivities for both homogeneous and atmospheric paths. In both cases the results were obtained by direct integration with respect to frequency. The homogeneous path calculations were compared with laboratory measurements and conclusions drawn concerning band strengths. The atmospheric path calculations were compared with measurements made by the SIRS instrument.

1. Introduction

The need for accurate transmissivity calculations for atmospheric paths in the 15-micron spectral region, where most of the absorption is due to the carbon dioxide molecule, has become very important in recent years due to the interest in atmospheric probing using infrared radiation intercepted by satellites and for radiative transport calculations in planetary atmospheres. In order to calculate atmospheric transmissivities using the direct integration technique it is necessary to have available good estimates of certain basic molecular parameters for carbon dioxide; unfortunately a number of these parameters have contradictory values assigned to them. One of the main purposes of this research is to decide which values should be used and also to develop methods for calculating transmissivities for homogeneous and atmospheric paths by direct integration with respect to frequency.

2. Calculation of Rotational Line Positions and Intensities

2.1 Calculation of Rotational Line Positions

2.1.1 The Carbon Dioxide Molecule

Since carbon dioxide is a linear symmetric molecule, the theoretical evaluation of certain basic parameters is somewhat simplified. The infrared optical activity of a molecule depends on the change in its electric moment. Figure 2.1 shows the modes of vibration of the carbon dioxide molecule.

In mode ν_1 there is no change in the electric moment and consequently no vibration band corresponding to this mode. The ν_1 fundamental vibration may, however, be studied using the Raman effect. There are also no pure rotation lines for carbon dioxide since on rotation there will be no change in the dipole moment. The ν_2 vibration is the degenerate representation of two equal frequencies and is centered about 667.4 cm^{-1} (approximately 15- microns). This mode is sometimes called the bending mode. Since the ν_2 band has a strong Q-branch we know that the change in electric moment is perpendicular to the axis of symmetry. The fundamental associated with the ν_3 mode is centered about 2349.2 cm^{-1} (approximately 4.3 microns). The Q-branch associated with this band is very weak indicating that the change in electric moment is parallel to the axis of symmetry. This mode is sometimes called the valence mode.

The above discussion applies to the symmetric isotopes such as $^{12}\text{C } ^{16}\text{O}_2$, $^{13}\text{C } ^{16}\text{O}_2$; if we consider isotopes such as $^{12}\text{C } ^{16}\text{O } ^{18}\text{O}$ or $^{12}\text{C } ^{16}\text{O } ^{17}\text{O}$ then we have destroyed some of the symmetry and we will see later how this influences our calculations.





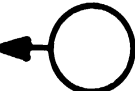
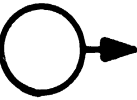
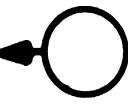




Change in Electric Moment	Oxygen	Carbon	Oxygen	Mode
None				ν_1
				ν_2
				ν_3

Figure 2.1. Vibrations of the carbon dioxide molecule and changes in electric moment.

The unperturbed energy levels may be calculated using the following formula (Courtoy, 1959),

$$\begin{aligned}
 G(v_1, v_2, v_3; \ell) = & \sum_{i=1}^3 \omega_i (v_i + d_i/2) \\
 & + \sum_{i=1}^3 \sum_{j \geq i} x_{ij} (v_i + \frac{d_i}{2}) (v_j + \frac{d_j}{2}) \\
 & + g_{22} \ell^2 + \sum_{i=1}^3 \sum_{j \geq i} \sum_{k \geq j} y_{ijk} (v_i + \frac{d_i}{2}) (v_j + \frac{d_j}{2}) (v_k + \frac{d_k}{2})
 \end{aligned} \tag{2.1.1}$$

where v_i are the vibrational quantum numbers, ℓ is a quantum number associated with the degeneracy of the v_2 - mode and gives the angular momentum (in units of $h/2\pi$) of the molecule about the symmetry axis of the degenerate vibration, d_i is a degeneracy index associated with the v_i - mode (for CO_2 we have, $d_1 = d_3 = 1$ and $d_2 = 2$) and the ω_i are the vibrational frequencies (in cm^{-1}). The vibrational constants ω_i , x_{ij} , y_{ijk} and g_{22} are generally determined experimentally. Formula (2.1.1) enables the energy levels to be calculated with respect to the minimum energy level.

Each vibration band is composed of a large number of spectral lines produced by the rotation of the molecule. The rotational energy levels are given by (Courtoy, 1959).

$$F(J) = BJ(J+1) - DJ^2(J+1)^2 \tag{2.1.2}$$

where B is the rotational constant and is related to the moment of inertia of the molecule, the term involving D takes into account the centrifugal stretching of the molecule and J is the rotational quantum number.

Courtoy (1959) gives a formula for B in terms of certain constants which are experimentally determined. .

$$B_{v_1 v_2 v_3} = B_{000} - \sum_{i=1}^3 \alpha_i v_i + \sum_{i=1}^3 \sum_{j \geq i}^3 \gamma_{ij} v_i v_j \quad (2.1.3)$$

where B_{000} is the rotational constant corresponding to level of lowest energy, viz. the level $(0, 0, 0: 0)$

The total energy for the molecule is thus given by

$$T(v_1, v_2, v_3: \ell: J) = G(v_1, v_2, v_3: \ell) + F(J) \quad (2.1.4)$$

We note that for degenerate vibrational levels (π, Δ, \dots) J must be larger or equal to ℓ viz.

$$J = \ell, \ell + 1, \ell + 2, \dots \quad (2.1.5)$$

The rotational levels of linear molecules are positive or negative depending on whether the total eigenfunction does not change sign or changes sign for an inversion. In the case of CO_2 the ground state is a \sum_g^+ state and the even rotational levels are positive with the odd levels negative. Also for CO_2 the positive rotational levels are symmetric and the negative anti-symmetric with respect to an interchange of all pairs of identical nuclei. The ratio of the statistical weights of the symmetrical and antisymmetrical rotational levels is determined by the nuclear spins. For the symmetric CO_2 isotopes, such as $^{12}\text{C} \ ^{16}\text{O}_2$, $^{13}\text{C} \ ^{16}\text{O}_2$, the antisymmetric levels have

weight zero while for the antisymmetric isotopes, such as $^{12}\text{C } ^{16}\text{O } ^{18}\text{O}$, $^{12}\text{C } ^{16}\text{O } ^{17}\text{O}$, the symmetric and antisymmetric levels have equal weight i. e. there is no distinction between symmetric and antisymmetric rotational levels.

Certain secondary effects must be considered, they are centrifugal stretching, Coriolis interaction, ℓ -type doubling and Fermi resonances. We noted previously the influence that centrifugal stretching has on the rotational energy levels.

The Coriolis vibration - rotation interaction is due to the rotation of the molecule and leads to a coupling between rotation and vibration. It also influences the intensity distribution of the rotational lines in a particular band. If we determine our rotational constants experimentally then we automatically take it into account.

The π, Δ, \dots vibrational levels of linear polyatomic molecules are doubly degenerate due to the equivalence of the two directions of the angular momentum. The interaction between the vibration and rotation slightly splits the degenerate levels giving ℓ -type doubling. It is thus necessary to consider different rotational constants for the split levels.

In a molecule, such as CO_2 , it often happens that two vibrational levels belonging to different vibrations may have almost the same energy. The two levels are in "resonance" and we obtain a perturbation of the energy levels. This is known as Fermi resonance.

For further discussion of the above topics Herzberg (1945) and Allen and Cross (1963) should be consulted.

In the next section we discuss the formulae and constants used to calculate the rotational line positions.

2.1.2 Rotational Line Positions

Equation (2.1.4) was used to calculate the rotational energy levels. To use this equation it was necessary to have available the vibrational energy levels and rotational constants. Tables 2.1 and 2.2 list the values used and their source. Fermi resonances, ℓ -type doubling and centrifugal stretching have been taken into account. The rotational constants have the superscripts c and d, using Courtoy's (1959) notation, corresponding to levels with even J positive or odd J positive, respectively.

The following isotopes have been considered $^{12}\text{C } ^{16}\text{O}_2$, $^{13}\text{C } ^{16}\text{O}_2$, $^{12}\text{C } ^{16}\text{O } ^{18}\text{O}$, $^{12}\text{C } ^{16}\text{O } ^{17}\text{O}$, $^{13}\text{C } ^{16}\text{O } ^{18}\text{O}$. Not all the bands for these molecules have been considered, only the stronger weighted by the isotopic abundance (ref. Section 2.2).

The possibility that the traditional assignments of ν_1 and $2\nu_2$ in $^{12}\text{C } ^{16}\text{O}_2$ should be reversed has been discussed by Amat and Pimbert (1965). They concluded that more study was needed. However, very recently Gordon and McCubbin (1966) have confirmed that the assignments of ν_1 and $2\nu_2$ should be reversed. Most of our calculations were completed when this information became available and we felt that we should continue our calculations rather than recalculate our line positions based on this information. The corrections involved are probably small.

TABLE 2.1. Vibrational energy levels for carbon dioxide in the 12-
18-micron region (units cm^{-1})

2.1a: Isotope $^{12}\text{C } ^{16}\text{O}_2$

LEVEL		G		ν_o
Lower	Upper	Lower	Upper	
000:0	010:1		667.379 ⁽¹⁾	667.379
010:1	020:0	667.379 ⁽¹⁾	1285.412 ⁽¹⁾	618.033
010:1	100:0	667.379 ⁽¹⁾	1388.187 ⁽¹⁾	720.808
010:1	020:2	667.379 ⁽¹⁾	1335.129 ⁽¹⁾	667.750
020:0	030:1	1285.412 ⁽¹⁾	1932.466 ⁽¹⁾	647.054
020:0	110:1	1285.412 ⁽¹⁾	2076.859 ⁽¹⁾	791.447
020:2	030:1	1335.129 ⁽¹⁾	1932.466 ⁽¹⁾	597.337
020:2	110:1	1335.129 ⁽¹⁾	2076.859 ⁽¹⁾	741.730
020:2	030:3	1335.129 ⁽¹⁾	2003.28 ⁽²⁾	668.151
100:0	030:1	1388.187 ⁽¹⁾	1932.466 ⁽¹⁾	544.279
100:0	110:1	1388.187 ⁽¹⁾	2076.859 ⁽¹⁾	688.672
030:3	040:2	2003.28 ⁽²⁾	2584.9 ⁽²⁾	581.62
030:3	120:2	2003.28 ⁽²⁾	2760.75 ⁽²⁾	757.47
030:1	120:2	1932.466 ⁽¹⁾	2760.75 ⁽²⁾	828.284
030:1	120:0	1932.466 ⁽¹⁾	2670.83 ⁽³⁾	738.364

2.1b: Isotope $^{13}\text{C } ^{16}\text{O}_2$

LEVEL		G		ν_o
Lower	Upper	Lower	Upper	
000:0	010:1		648.52 ⁽¹⁾	648.52
010:1	020:0	648.52 ⁽¹⁾	1265.81 ⁽¹⁾	617.29
010:1	100:0	648.52 ⁽¹⁾	1370.05 ⁽¹⁾	721.53
010:1	020:2	648.52 ⁽¹⁾	1297.40 ⁽¹⁾	648.88
020:0	030:1	1265.81 ⁽¹⁾	1896.54 ⁽¹⁾	630.73
020:2	030:3	1297.40 ⁽¹⁾	1946.69 ⁽²⁾	649.29
100:0	110:1	1370.05 ⁽¹⁾	2037.11 ⁽¹⁾	667.06

2.1c: Isotope $^{12}\text{C } ^{16}\text{O } ^{18}\text{O}$

LEVEL		G		ν_o
Lower	Upper	Lower	Upper	
000:0	010:1		662.29 ⁽¹⁾	662.29
010:1	020:0	662.29 ⁽¹⁾	1365.84 ⁽¹⁾	703.55
010:1	100:0	662.29 ⁽¹⁾	1259.43 ⁽¹⁾	597.14
010:1	020:2	662.29 ⁽¹⁾	1325.01 ⁽²⁾	662.72
020:0	030:1	1365.84 ⁽¹⁾	2049.25 ⁽²⁾	683.41

(1) Gordon and McCubbin (1965)

(2) Courtoy (1959)

(3) Stull, Wyatt and Plass (1962)

2.1d: Isotope $^{12}\text{C } ^{16}\text{O } ^{17}\text{O}$

LEVEL		G		ν_o
Lower	Upper	Lower	Upper	
000:0	010:1		664.72 ⁽³⁾	664.72
010:1	020:2	664.72 ⁽³⁾	1329.79 ⁽³⁾	665.07

2.1e: Isotope $^{13}\text{C } ^{16}\text{O } ^{18}\text{O}$

LEVEL		G		ν_o
Lower	Upper	Lower	Upper	
000:0	010:1		643.49 ⁽³⁾	643.49

TABLE 2.2. Rotational constants for carbon dioxide in the 12 to 18-micron region (units cm^{-1})

2.2a: Isotope $^{12}\text{C } ^{16}\text{O}_2$

Level	B^c	B^d	D^c	D^d	
000:0	0.39021	0.39021	13.5×10^{-8}	13.5×10^{-8}	(3)
010:1	0.390635	0.391245	13.8×10^{-8}	13.7×10^{-8}	(1)
020:0	0.390476	0.390476	16.1×10^{-8}	16.1×10^{-8}	(1)
100:0	0.390201	0.390201	12.8×10^{-8}	12.8×10^{-8}	(1)
020:2	0.391657	0.391657	13.9×10^{-8}	13.7×10^{-8}	(1)
030:1	0.390756	0.391675	14×10^{-8}	14.6×10^{-8}	(1)
110:1	0.390372	0.391326	12×10^{-8}	10.6×10^{-8}	(1)
030:3	0.39236	0.39236	13×10^{-8}	13×10^{-8}	(2)
120:0	0.388525	0.388525	13×10^{-8}	13×10^{-8}	(3)
040:2	0.39187	0.39187	13×10^{-8}	13×10^{-8}	(3)
120:2	0.39152	0.39152	12.2×10^{-8}	12.2×10^{-8}	(2)

2.2b: Isotope $^{13}\text{C } ^{16}\text{O}_2$

Level	B^c	B^d	D^c	D^d	
000:0	0.39025	0.39025	13.7×10^{-8}	13.7×10^{-8}	(3)
010:1	0.39064	0.39126	13.7×10^{-8}	13.7×10^{-8}	(3)
020:0	0.390935	0.390935	15.9×10^{-8}	15.9×10^{-8}	(3)
100:0	0.389745	0.389745	12.2×10^{-8}	12.2×10^{-8}	(3)
020:2	0.39165	0.39165	13.3×10^{-8}	13.3×10^{-8}	(3)
030:1	0.39090	0.39216	13×10^{-8}	13×10^{-8}	(3), (4)
110:1	0.39023	0.39084	13×10^{-8}	13×10^{-8}	(3), (4)
030:3	0.39096	0.39096	13×10^{-8}	13×10^{-8}	(3), (4)

2.2c: Isotope $^{12}\text{C}^{16}\text{O}^{18}\text{O}$

Level	B^c	B^d	D^c	D^d	
000:0	0.36820	0.36820	11.5×10^{-8}	11.5×10^{-8}	(3)
010:1	0.36857	0.36912	11.5×10^{-8}	11.5×10^{-8}	(5)
020:0	0.36851	0.36851	11×10^{-8}	11×10^{-8}	(5)
100:0	0.36811	0.36811	11×10^{-8}	11×10^{-8}	(5)
020:2	0.36948	0.36948	11×10^{-8}	11×10^{-8}	(5)
030:1	0.36924	0.37008	11×10^{-8}	11×10^{-8}	(5)

2.2d: Isotope $^{12}\text{C}^{16}\text{O}^{17}\text{O}$

Level	B^c	B^d	D^c	D^d	
000:0	0.37922	0.37922	12.5×10^{-8}	12.5×10^{-8}	(6)
010:1	0.37826	0.37884	12.5×10^{-8}	12.5×10^{-8}	(7)
020:2	0.37923	0.37923	12.5×10^{-8}	12.5×10^{-8}	(7)

2.2e: Isotope $^{13}\text{C}^{16}\text{O}^{18}\text{O}$

Level	B^c	B^d	D^c	D^d	
000.0	0.36820	0.36820	11.5×10^{-8}	11.5×10^{-8}	(3)
010:1	0.36727	0.36785	11.5×10^{-8}	11.5×10^{-8}	(5)

- (1). These values were obtained from the values given by Gordon and McCubbin (1965) using Courtoy's (1959) values for the 000:0 level as a base value.
- (2). Benedict (1957).
- (3). Courtoy (1959).
- (4). The D's were calculated using $D = 4 B_e^3 / \nu_1^2$
- (5). Calculated using Courtoy's (1959) constants, Fermi resonances were taken into account in the calculations.
- (6). The rotational constants were obtained by linear interpolation using the other isotopes as base values.
- (7). Calculated using interpolated parameters.

2.2 Calculation of Rotational Line Intensities

The intensity of an individual rotational line is given by (cf. Penner, 1959).

$$S(n_1'', n_2'', n_3'' : \ell'' : J'' \longrightarrow n_1', n_2', n_3' : \ell' : J')$$

$$= \frac{8\pi^3 \nu N(T)}{3hc Q_V Q_J} \left(\exp - \frac{T(n_1'', n_2'', n_3'' : \ell'' : J'')}{kT} \right) \quad (2.2.1)$$

$$\times g_{J'\ell'} (A_{J''\ell''}^{J'\ell'})^2 \beta^2 (1 - \exp(-\frac{h\nu}{kT}))$$

where ' refers to the upper level, '' to the lower level and ν is the frequency (cm^{-1}) corresponding to the indicated change in quantum numbers. $N(T)$ is the number of molecules per unit volume per unit pressure at temperature T . $g_{J'\ell'}$ is the statistical weight of the upper level given by

$$g_{J'\ell'} = 2J' + 1 \text{ for } \ell' = 0$$

$$g_{J'\ell'} = 2(2J' + 1) \text{ for } \ell' \neq 0$$

β is an empirical factor corresponding to the matrix elements.

Q_J is the complete rotational partition function.

Q_V is the complete vibrational partition function.

$(A_{J''\ell''}^{J'\ell'})$ are the amplitude factors listed in Table 3.

$T(n_1'', n_2'', n_3'' : \ell'' : J'')$ is the energy of the lower level.

TABLE 3. Amplitude Factors

(Penner, 1959: Dennison, 1931)

$$(A_{J'' 1}^{J'' 0})^2 = 1/2$$

$$\Delta J = 0, \Delta \ell = -1$$

$$(A_{J''-1 1}^{J'' 0})^2 = \frac{J''-1}{2(2J''+1)}$$

$$\Delta J = +1, \Delta \ell = -1$$

$$(A_{J'' 1}^{J''-1 0})^2 = \frac{J''+1}{2(2J''-1)}$$

$$\Delta J = -1, \Delta \ell = -1$$

$$(A_{J'' \ell'' \mp 1}^{J'' \ell''})^2 = \frac{(J'' \pm \ell'') (J'' \mp \ell'' + 1)}{4J'' (2J'' + 1)}$$

$$\ell'' \neq 0, \Delta \ell = \pm 1$$

$$\Delta J = 0$$

$$(A_{J''-1 \ell'' \mp 1}^{J'' \ell''})^2 = \frac{(J'' \pm \ell'') (J'' \pm \ell'' - 1)}{4J'' (2J'' + 1)}$$

$$\ell'' \neq 0, \Delta \ell = \pm 1$$

$$\Delta J = +1$$

$$(A_{J'' \ell'' \mp 1}^{J''-1 \ell''})^2 = \frac{(J'' \pm \ell'') (J'' \pm \ell'' + 1)}{4J'' (2J'' - 1)}$$

$$\ell'' \neq 0, \Delta \ell = \pm 1$$

$$\Delta J = -1$$

The intensity of a band is given by (cf. Penner, 1959).

$$\begin{aligned}
 & S(n_1'', n_2'', n_3'' : \ell'' \longrightarrow n_1', n_2', n_3' : \ell') \\
 &= \frac{4\pi^3 \beta^2 \nu_0 N(T)}{3hc Q_V} g_{\ell''} \left(\exp \frac{-G(n_1'', n_2'', n_3'' : \ell'')}{kT} \right) \quad (2.2.2) \\
 & \quad \times \left(1 - \exp \left(-\frac{hc \nu_0}{kT} \right) \right)
 \end{aligned}$$

where ν_0 is the frequency corresponding to the band center

$G(n_1'', n_2'', n_3'' : \ell)$ is the vibrational energy

and $g_{\ell''} = 1$ for $\ell'' = 0$

$g_{\ell''} = 2$ for $\ell'' \neq 0$

We calculate β^2 from (2.2.2) and substitute into (2.2.1) to give

$$\begin{aligned}
 & S(n_1'', n_2'', n_3'' : \ell'' J'' \longrightarrow n_1', n_2', n_3' : \ell' J') \\
 &= \frac{2g_{J'\ell'} (A_{J''\ell''}^{J'\ell'})^2 S(T) \nu (1 - \exp(-\frac{hc\nu}{kT})) \exp(-\frac{F(J'', \ell'')}{kT})}{g_{\ell''} Q_J \nu_0 (1 - \exp(-\frac{hc\nu_0}{kT}))} \quad (2.2.3)
 \end{aligned}$$

where $S(T)$ is the band intensity and $F(J'', \ell'')$ is the rotational energy level.

Now, in addition, we have

$$\frac{S(T)}{S(T_0)} = \frac{N(T) Q_v(T_0) (1 - \exp(-hc \nu_0/kT))}{N(T_0) Q_v(T) (1 - \exp(-hc \nu_0/kT_0))} \quad (2.2.4)$$

If we keep the pressure constant then

$$\frac{N(T)}{N(T_0)} = \frac{T_0}{T}$$

and consequently

$$\frac{S(T)}{S(T_0)} = \frac{T_0 Q_v(T_0) (1 - \exp(-hc \nu_0/kT))}{T Q_v(T) (1 - \exp(-hc \nu_0/kT_0))} \quad (2.2.5)$$

Therefore

$$\begin{aligned} S(n_1'', n_2'', n_3'': \ell'': J'') &\longrightarrow n_1', n_2', n_3': \ell': J') \\ &= \frac{2g_{J', \ell'} (A_{J'', \ell''}^{J', \ell'})^2 \nu S(T_0) T_0 Q_v(T_0) (1 - \exp(-hc \nu/kT))}{g_{\ell''} Q_J(T) \nu_0 T Q_v(T) (1 - \exp(-hc \nu_0/kT_0))} \quad (2.2.6) \end{aligned}$$

$$\times \exp(-F(J'', \ell'')/kT)$$

The above discussion is applicable to the symmetric molecules such as $^{12}\text{C } ^{16}\text{O}_2$, $^{13}\text{C } ^{16}\text{O}_2$. For non-symmetric molecules such as $^{12}\text{C } ^{16}\text{O } ^{18}\text{O}$ it is necessary to take $g_{\ell''}$ as 2 for all values of ℓ'' since the symmetric and anti-symmetric levels are all occupied.

For $^{12}\text{C}^{16}\text{O}_2$ the partition functions were calculated by interpolation on the values given by Gray and Selvidge (1965). In the case of the remaining isotopes the partition functions were calculated using the harmonic oscillator partition functions (Herzberg, 1945).

$$Q_v = \prod_{i=1}^3 (1 - \exp(-hc \nu_i^{\circ}/kT))^{-d_i} \quad (2.2.7)$$

where d_i are the degrees of degeneracy of the vibrations ν_i° , and

$$Q_J = \frac{kT}{hc B_e} + \frac{1}{3} + \frac{1}{15} \frac{hc B_e}{kT} + \frac{4}{315} \left(\frac{hc B_e}{kT} \right)^2 + \frac{1}{315} \left(\frac{hc B_e}{kT} \right)^3 + \dots \quad (2.2.8)$$

A program was written which computed the rotational line intensities for the various bands in the 12 to 18 micron region. The isotopes $^{12}\text{C}^{16}\text{O}_2$, $^{13}\text{C}^{16}\text{O}_2$, $^{12}\text{C}^{16}\text{O}^{18}\text{O}$, $^{12}\text{C}^{16}\text{O}^{17}\text{O}$, $^{13}\text{C}^{16}\text{O}^{18}\text{O}$ were considered. The band intensities for the various isotopes were weighted by their abundance, which can be calculated using the isotopic abundances of carbon and oxygen. They are:

$^{12}\text{C}^{16}\text{O}_2$	1.00
$^{13}\text{C}^{16}\text{O}_2$	1.12×10^{-2}
$^{12}\text{C}^{16}\text{O}^{18}\text{O}$	4.0×10^{-3}
$^{12}\text{C}^{16}\text{O}^{17}\text{O}$	8.0×10^{-4}
$^{13}\text{C}^{16}\text{O}^{18}\text{O}$	4.5×10^{-5}

A check on the accuracy of the rotational line intensities is to calculate the rotational line intensities for each band, then add the individual line intensities together. The results should agree closely with the original band intensity. This calculation was performed and is discussed in Section 4 where the selection of suitable band intensities is discussed.

3. Direct Integration Techniques

3.1 Introduction

Suppose that we have a sample of gas which contains one or more optically absorbing constituents. The transmissivity at any frequency along a given path is a function of both the position and the intensity of the individual absorption lines, as well as the physical characteristics of the sample (temperature, pressure, concentration, etc.). Inhomogenities introduce additional complications to the determination of transmissivity. It is the purpose of this chapter to describe in some detail the methods by which the absorption has been calculated, with particular emphasis on paths through the atmosphere.

For theoretical or experimental purposes, we are generally interested in obtaining the transmissivity $\bar{\gamma}$ averaged over a finite frequency interval $\Delta\nu$, weighted by some function $\phi(\nu)$

$$\bar{\gamma} = \frac{\int_{\Delta\nu} \phi(\nu) \gamma_{\nu} d\nu}{\int_{\Delta\nu} \phi(\nu) d\nu} \quad (3.1.1a)$$

In the case of a spectrometer with slit function $\omega(\nu)$, we calculate

$$\gamma_{\nu^*} = \frac{\int_{\nu_1}^{\nu_2} \omega(\nu^* - \nu) \gamma_{\nu} d\nu}{\int_{\nu_1}^{\nu_2} \omega(\nu^* - \nu) d\nu} \quad (3.1.1b)$$

i.e., the weighting function $\phi(\nu)$ is equal to the slit function $\omega(\nu^* - \nu)$

It is theoretically possible to use standard quadrature techniques to calculate $\bar{\gamma}$ to any desired accuracy, provided that we can obtain γ_{ν} at any frequency in the integration interval. However, γ_{ν} typically includes contributions from many spectral lines and because it is a rapidly varying function of frequency, we need many calculations for even

a small frequency interval. This precludes hand calculations for all but the simplest situations. Band models were introduced to overcome this difficulty. Using a band model allows one to suitably approximate the true distribution and intensities of the spectral lines in such a manner that analytic expressions for $\bar{\gamma}$ can be obtained, at least, in the case where the weighting function $\phi(\nu)$ is constant. Several such models of varying complexity and realism have been used (see Goody (1964), Plass (1958) and Drayson (1964), for details). These band models were very important in the development and application of radiative transfer theory, particularly for meteorological applications.

In recent years the rapid advancements in the field of digital computing have made the numerical evaluation of Eq. 3.1.1 an attractive alternative. Several successful calculations using this approach have been made for infrared active molecules in the atmosphere. [Hitschfeld and Houghton (1961), Shaw and Houghton (1964), Gates et al. (1963), Gates and Calfee (1966), Drayson (1966).] The results have shown that the same input data may yield substantial differences when the absorption from a band model is compared with the absorption obtained by direct integration [Drayson (1964) and (1966)].

Because of the errors introduced by band models it has been rather difficult to obtain some of the basic band parameters needed for the calculation of absorption. Of these parameters the two most important are the total band intensity and the Lorentz half-width. In a later section it is shown how the direct integration techniques may be used as a tool to deduce more accurate values.

3.2 Homogeneous Paths

The transmissivity γ_ν for monochromatic radiation at frequency ν is given by

$$\gamma_\nu = \exp \left(- \int k_\nu du \right) \quad (3.2.1)$$

where k_ν is the absorption coefficient and u is the optical mass, the integral being taken along the absorption path. In general the pressure, temperature and other parameters will change along the path.

The absorption coefficient k_ν may be expressed as the sum of absorption coefficients of the individual spectral lines.

$$k_\nu = \sum_i k_\nu(i) \quad (3.2.2)$$

The value of $k_\nu(i)$ depends on the shape of the spectral line. For the 15μ bands of CO_2 there are three line shapes of importance.

- a) Lorentz line shape, in regions where pressure or collisional broadening dominates.

$$k_\nu(i) = \frac{S_i}{\pi} \frac{\alpha_L(i)}{(\nu - \nu_i)^2 + (\alpha_L(i))^2} \quad (3.2.3)$$

where S_i is the intensity of the i^{th} line

$\alpha_L(i)$ the Lorentz half-width

ν_i the frequency of the line center

b) Doppler line shape

$$k_{\nu}(i) = k_o(i) \exp(-x^2) \quad (3.2.4)$$

where

$$x = \frac{(\nu - \nu_i)}{\alpha_D} \sqrt{\ln 2}$$

α_D is the Doppler half-width

$$k_o = \frac{S_i}{\alpha_D} \sqrt{\frac{\ln 2}{\pi}}$$

c) Mixed Doppler-Lorentz line shape

$$k_{\nu}(i) = \frac{k_o y}{\pi} \int_{-\infty}^{+\infty} \frac{e^{-t^2}}{y^2 + (x-t)^2} dt \quad (3.2.5)$$

where

$$y = \frac{\alpha_L(i)}{\alpha_D} \sqrt{\ln 2}$$

Strictly speaking, the mixed Doppler-Lorentz line shape should be used at all pressures, but at higher pressures where the Lorentz half width is much greater than the Doppler, the error in using Lorentz broadening is quite small. Similarly, at very low pressures Doppler broadening is adequate. For the calculations described in this report, the Lorentz line shape was employed at pressures higher than 0.1 atmosphere, and the mixed Doppler-Lorentz at all lower pressures (Drayson (1966)).

As a special case, consider a homogeneous absorption path, i. e. one along which the physical parameters are kept constant. Such conditions are nearly always used in experimental laboratory measurements, and are therefore of great interest and importance, as well as being simplest to calculate. Eq. (3.2.1) reduces to

$$\gamma_{\nu} = \exp(-k_{\nu} u) \quad (3.2.6)$$

k_{ν} may be readily evaluated from Eq. (3.2.2) using the appropriate line shape. Standard quadrature techniques are used to evaluate (3.1.1)

3.3 Slant Paths

In meteorological and other atmospheric applications we are seldom fortunate enough to encounter homogeneous absorption paths. Variations in temperature and pressure, and hence in half-width (Doppler and Lorentz) and in line intensity, must be accounted for in the evaluation of the integral

$$\tau_{\nu}(i) = \int k_{\nu}(i) du \quad (3.3.1)$$

Suppose the atmosphere is divided into horizontal layers, with only a small variation of temperature within the layer. By treating the layer as isothermal and assuming a constant mixing ratio for CO_2 , it is possible to obtain expressions for Eq. (3.3.1) (Drayson 1966).

For Lorentz broadening

$$\tau_{\nu(i)} = \frac{c S_i}{\alpha \pi \alpha_o} \ln \left[\frac{\alpha_o^2 p_2^2 + (\nu - \nu_i)^2}{\alpha_o^2 p_1^2 + (\nu - \nu_i)^2} \right] \quad (3.3.2)$$

where p_1 and p_2 are the pressures of the upper and lower boundaries, α_o is defined by the relation $\alpha_L(i) = \alpha_o p$, within the layer and

$$c = \frac{dp}{du}$$

The corresponding expression for the mixed Doppler-Lorentz broadening is more complicated

$$\tau_{\nu(i)} = \int_{-\infty}^{+\infty} \int_{p_1}^{p_2} \frac{k_o y c}{\pi} \frac{e^{-t^2}}{y^2 + (x - t)^2} dp dt \quad (3.3.3)$$

The result of integrating with respect to pressure is

$$\tau_{\nu(i)} = \frac{k_o c}{2 \pi y_o} \int_{-\infty}^{\infty} e^{-t^2} \ln \left[\frac{y_o^2 p_2^2 + (x-t)^2}{y_o^2 p_1^2 + (x-t)^2} \right] dt \quad (3.3.4)$$

where y is defined by $y = y_o p$

The value of τ_{ν} for a path between two points in the atmosphere is obtained by summing $\tau_{\nu(i)}$ over the absorption lines and over the pressure layers between the points.

It is a frequent practice to reduce the absorption over a variable slant path to a homogeneous path by means of the Curtis-Godson approximation. This method is sometimes quite satisfactory, but can lead to absorption errors as high as 6%. However, these errors can be sharply reduced by approximating the atmosphere by not one but several homogeneous layers, applying the Curtis-Godson approximation over each of these. This method was applied by Gates and Calfee (1966) to atmospheric water vapor absorption.

3.4 Programing Techniques

The transmissivity $\bar{\gamma}$ defined by Eq. (3.1.1) may be readily evaluated by standard quadrature procedures. However, to carry out this task in an efficient manner and produce accurate answers over a wide variety of physical conditions is not a trivial problem. In the course of writing the computer programs a large number of techniques and approximations were investigated before being incorporated into the programs. It is the purpose of this section to describe some of these techniques which may prove useful to others writing similar programs.'

In evaluating the integral of some function over a finite interval, it is generally more efficient to apply low order quadrature over a number of sub-intervals, rather than higher order quadrature over the whole interval. This is particularly important when the integrand is a rapidly fluctuating function of the integration variable. The evaluation of the integral

$$\bar{\gamma} = \int_{\nu_1}^{\nu_2} \gamma_{\nu} d\nu \quad (3.4.1)$$

is an excellent example. In the neighborhood of a line centre, the value of γ_v may be almost zero while remaining near unity away from the line. Moreover, the neighborhood of the line centre may be quite narrow with a very rapid change from complete absorption to negligible absorption. By a process of trial and error it was found that the integration near the line centre could be accomplished by 4-point Gaussian quadrature over intervals formed by points distance 0.0, 0.001, 0.002, 0.003, 0.005 and 0.01 cm^{-1} from the line centre. Higher order quadrature resulted in no differences in $\bar{\gamma}$ in the 6th decimal place. Lower order quadrature led to a rapid deterioration, particularly at lower pressures. It should be noted at this point that the consideration of mixed Doppler-Lorentz broadening is an asset rather than a hinderance in choosing the interval subdivision. If pure Lorentz broadening is used at low pressures the line profile becomes very sharp and smaller subdivisions must be employed. Doppler-Lorentz broadening limits the line half-width to about $6 \times 10^{-4} \text{ cm}^{-1}$, even at very low pressures.

In the gaps between the spectral lines the procedure is not so clear-cut. Using 4-point Gaussian quadrature over intervals of length 0.01 cm^{-1} gave convergent solutions, but is wasteful since a much coarser subdivision is sufficient. A modified form of this, using 0.01 $^{-1}$ sub-intervals out of 0.04 or 0.05 cm^{-1} from the line centres and 0.1 cm^{-1} sub-intervals elsewhere proved adequate, as did one or two similar methods.

In the course of testing the programs it was found that round off error in the machine's representation and manipulation of the frequencies

of the lines and of the quadrature points could introduce considerable noise. This difficulty was overcome in the following way: the line frequencies were read into two decimal places, multiplied by 100 and converted from floating point to integer mode. To calculate the absorption in any 1 cm^{-1} interval, the frequencies were converted back to floating point, relative to the center of the interval. By calculating all frequencies relative to this point, the difference between neighboring frequencies could be accurately found.

The mixed Doppler-Lorentz integral in Eq. (3.2.5) was calculated using the method described by Young (1965), with one modification: 4-point Gauss-Hermite quadrature was employed for $x \geq 7.0$, instead of 20-point Gauss-Hermite quadrature for $x \geq 10.0$. The same accuracy was maintained with a considerable saving in execution time.

In the present calculations the half-width was assumed to be the same for all lines, enabling a further simplification to be made. Since the Doppler half-width is directly proportional to frequency, it varies only slightly over a 1 cm^{-1} interval. By taking the value of half-width at the centre of the interval, the integral (3.2.5) was evaluated for those values of x and y corresponding to the quadrature points in the neighborhood of a line centre (i.e. within 0.01 of the line centre), for each pressure being calculated. (For slant paths the integral is (3.3.3)). These values, multiplied by the appropriate line intensity, can be used for all lines in the 1 cm^{-1} interval. This gives a considerable time saving, especially in those regions (eg. Q-branches) where the line distribution is dense.

In addition, the value of x is small for frequencies near the line centre, and it is the small values of x which take the longest time to calculate.

The Lorentz line shape is used for $|\nu - \nu_i| \geq 0.2$.

The above method was further extended to cover those values of $|\nu - \nu_i|$ satisfying $0.2 \geq |\nu - \nu_i| \geq 0.1$. A useful reduction in execution time was obtained in the Q-branches, with smaller savings elsewhere.

Let us now consider a 1 cm^{-1} interval in which transmission calculations are being made. Those lines which are distant from the interval normally contribute only a small amount to the absorption; furthermore their contribution does not vary very much over the interval. Instead of computing their contribution directly at each quadrature point, it is calculated only at the centre and two end points of the 1 cm^{-1} interval. Lagrange interpolation is used at intermediate points. More specifically, the Lorentz line shape is approximated by

$$\frac{\alpha_L}{\pi} \frac{S_i}{(\nu - \nu_i)^2}$$

and the sum
$$\sum_i \frac{S_i}{(\nu - \nu_i)^2}$$

formed, with the index i running over those lines further than some distance, d_0 say, from the interval centre. Test calculations in the $15\mu \text{ CO}_2$ bands showed that $d_0 = 3.5 \text{ cm}^{-1}$ produced no errors out to the 6th significant figure. Smaller values led to rapid deterioration. The sum above must be multiplied by α_L/π , using the correct value of α_L for the temperature and

pressure under consideration. For the slant paths, where the temperature varies, the sum was formed for 6 temperatures, and interpolated for the correct temperature value.

The same sort of interpolative procedure may be used over a 0.1 cm^{-1} interval. In this case the sum

$$\sum_i k_\nu(i)$$

is formed at each pressure, for those lines at distance greater than or equal to some minimum, say d_1 , from the centre of the 0.1 cm^{-1} interval. Similar tests showed $d_1 = 0.8 \text{ cm}^{-1}$ to be a satisfactory value.

Finally, on the smallest scale the interpolation technique may be used in a line neighborhood, ± 0.01 from the line centre. The sum

$$\sum_i k_\nu(i)$$

was again formed, for lines greater than d_2 from the line centre. A value of $d_2 = 0.1 \text{ cm}^{-1}$ proved adequate.

These three interpolative procedures are very important for efficient programing, especially the first. They enable the effect of all lines to be accurately included, without calculating directly their contribution at each quadrature frequency. However, the programing is necessarily more complicated using these techniques and requires careful checking.

Most of the programing was written in MAD language, which is very flexible and easy to use. The object program produced by MAD is not always very efficient, so that certain critical subroutines were rewritten in UMAP, an assembly program similar to FAP. For homogeneous paths, two completely separate programs were written by different programmers. When the

same input parameters were used, both programs gave the same answers to six significant figures, providing a good check on the accuracy. A further check was made by calculating the absorption due to a single isolated line with Lorentz line shape, using the programs developed and also using the Ladenburg—Reiche formula; the same accuracy was attained.

In making practical absorption calculations such high numerical accuracy is rarely, if ever, needed. Some of the convergence criterion were relaxed to produce a faster but slightly less accurate program. To give some indication of the speed of the program the following example is given. Input 2137 lines, transmissivity calculated at a resolution of 0.1 wave numbers for a total of 20 homogeneous paths at 4 pressures, three of which require mixed Doppler-Lorentz broadening, for the 390 cm^{-1} interval from 489.5 to 879.5 cm^{-1} . Time taken: about 58 minutes on an IBM 7090. The 5 cm^{-1} interval about the main Q-branch took just over 4 minutes. A typical 1 cm^{-1} interval in the main R-branch containing 5 absorption lines took about 6.5 seconds. These times compare quite favorably with execution times required for band models, where they can be applied.

The programs described were developed specifically for the 15μ region, but are quite general in scope and have also been used to calculate the absorption in other regions (eg, the oxygen A-band). Because the input parameters differ from band to band, the approximations should be re-tested for validity. Where a lower accuracy is sufficient, some of the conditions may be relaxed to give a faster calculation. The numerical errors in calculation are certainly negligible compared to the uncertainty in band intensities, half-widths and line shapes.

4. Homogeneous Path Transmissivities

4.1 Calculation of Rotational Line Positions and Intensities

We have discussed in Section 2 the methods for calculating the rotational line positions and strengths. In this section we will discuss the practical details of the computation.

The calculation of the rotational line positions poses no difficulty since the relevant parameters are fairly well known, the values listed in Section 2 were used.

The calculation of the rotational line intensities is, in principle, not difficult. However, we need to know accurate values for the band intensities, quantities which are not very well known. Determining accurate band intensities from experimental measurements is difficult, we will discuss this point later. The band intensities that we used are listed in Table 4.1. The integrated intensity for all the bands is $241.24 \text{ cm}^{-1} (\text{atm. cm})^{-1}$ at 300°K . It is interesting to compare this value with some of the estimates which have appeared in the literature. Table 4.2, taken in the most part from Varanasi and Lauer (1966), lists most of the recent estimates for the integrated band intensity. It is interesting to note the wide range of values quoted in the light of the various error estimates. The value that we used is a little higher than most of the estimates, we will discuss this point later.

In the present calculations we have neglected the influence of the Coriolis vibration-rotation interaction on the intensity distribution within a particular band. Due to the uncertainties in the band intensities we feel that attempting to introduce this additional correction is not justified, particularly since the necessary parameters are not too well known.

TABLE 4.1. Band Intensities Used in Calculating Rotational Line Intensities

LEVEL		BAND	INTENSITY
Lower	Upper	Center	(cm ⁻¹ (atm cm) ⁻¹ at 300°K)
000:0	010:1	667.379	194 ⁽¹⁾
010:1	020:0	618.033	4.27 ⁽¹⁾
010:1	100:0	720.808	6.2 ⁽²⁾
010:1	020:2	667.750	30 ⁽¹⁾
020:0	030:1	647.054	1.0 ⁽¹⁾
020:0	110:1	791.447	0.022 ⁽²⁾
020:2	030:1	597.337	0.14 ⁽¹⁾
020:2	110:1	741.730	0.14 ⁽²⁾
020:2	030:3	668.151	0.85 ⁽²⁾
100:0	110:1	688.672	0.3 ⁽³⁾
100:0	030:1	544.279	0.004 ⁽¹⁾
030:3	040:2	581.62	0.0042 ⁽²⁾
030:3	120:2	757.47	0.0059 ⁽²⁾
030:1	120:2	828.284	0.00049 ⁽²⁾
030:1	120:0	738.364	0.014 ⁽²⁾

(1) Madden (1961)

(2) Yamamoto and Sasamori (1958)

(3) Yamamoto and Sasamori (1964)

TABLE 4.2. Integrated Intensity of the 15 - Micron CO₂ Bands

	Integrated Intensity (cm ⁻¹ (atm. cm) ⁻¹ at 300°K)
Burch, Gryvnak and Williams (1962)	330 ± 90
Weber, Holm and Penner (1952)	170 ± 34
Kaplan and Eggers (1956)	217 ± 5
Thorndike (1947)	170 ± 18
Overend, Youngquist, Curtis and Crawford (1959)	218 ± 5
Schurin (1960)	217 ± 5
Eggers and Crawford (1951)	146 ± 18
Varanasi and Lauer (1966)	200 ± 10
National Environmental Satellite Lab., E. S. S. A., (1966)	225 ± 7

As we noted in Section 2, a check on the accuracy of the rotational line intensity calculation is to add together the calculated rotational line intensities in a given band; the result should equal the band intensity. This calculation was carried out for all the bands, excellent agreement being obtained.

In the calculation of the rotational line intensities we neglected lines with intensities less than $10^{-6} \text{ cm}^{-1} (\text{atm. cm})^{-1}$ at 300°K ; nevertheless, we ended up with about 7000 rotational lines. Since the calculation of transmissivities using this number of lines would be an exceedingly lengthy task, we decided to reduce the number of lines using a suitable criterion. Examination of the line intensities showed that most of the lines had intensities in the range 10^{-4} to $10^{-6} \text{ cm}^{-1} (\text{atm. cm})^{-1}$. Also near strong lines very weak lines would have little influence except at very low pressures. We divided the spectral range into 5 cm^{-1} intervals and retained only those lines with intensities lying in the range formed by the strongest line and 10^{-3} times the intensity of the strongest line in the interval. By imposing this criterion we reduced the number of rotational lines to around 2000, a more manageable number. The criterion we have used has the advantage that in spectral regions where there are only weak lines they are retained while in spectral regions with strong and weak lines we retain the strong lines and some of the weak lines, the very weak lines being neglected.

We performed the line intensity calculations for six temperatures 300, 275, 250, 225, 200 and 175°K . Intensities for other temperatures may be readily obtained by interpolation. This information has been stored on punched cards and is available, on request, in that form, or on magnetic tape, but is not reproduced in this report.

4.2 Half-Widths and Line Shapes

In order to calculate transmissivities, as noted in Section 3, we need to know the Lorentz or collisional half-width and the line shape.

The most generally used value for the nitrogen-broadened Lorentz half-width is 0.064 cm^{-1} at 1 atm. and 298°K (Kaplan and Eggers, (1956)). It is very difficult to obtain reliable values for the half-width from the technique used by Kaplan and Eggers (1956). In the case of self-broadened carbon dioxide the half-width varies with the rotational quantum number. Madden (1961) obtained a half-width of 0.126 cm^{-1} (1 atm., 300°K) for the $J = 4$ line of the P-branch of the ν_2 fundamental and 0.06 cm^{-1} for the $J = 56$ line of the same band and branch. Burch et al. (1965) also present some data on the variation of half-width with rotational quantum number for the CO_2 bands in the 1 to 1.25 micron region. They obtained a mean value of 0.10 cm^{-1} (1 atm., 300°K) for the self-broadened half-width which agrees quite well with the values given by Madden. If we use the self-broadening coefficient 1.3 given by Burch et al. (1962) then we obtain 0.077 cm^{-1} as the value for air-broadened CO_2 . It is interesting to note that Gray and McClatchey (1965) used a value of 0.07 cm^{-1} in their calculations involving the 4.3 micron bands, this value being provided by Kaplan. In the light of the above considerations we have used 0.08 cm^{-1} (1 atm., 300°K) for the Lorentz half-width, but in later calculations we intend to study the effect of changing this value. Because the variation of half-width with rotational quantum number for air-broadened CO_2 is not known at the moment, we used a constant value.

As noted in Section 3 we used the Lorentz line shape for pressures greater than 0.1 atm. and the Doppler-Lorentz (Voigt) profile for pressures

less than 0.1 atm. Winters et al. (1964) has discussed the departure of the line shape from Lorentzian in the wings of lines for self-broadened CO₂, they studied the 4.3 micron band. They concluded that the absorption in the wings of lines drops off more rapidly than calculated from the Lorentz formula. However since no results are available for the 15 μ region or for air (or nitrogen) broadened CO₂ we have used the Lorentz formula for the wings.

4.3 Comparison of Calculated and Experimental Transmissivities

The transmissivities for the homogeneous paths were calculated using the procedures outlined in Section 3. The pressures and optical masses for which the calculations were made were chosen to agree with those used by Burch et al. (1962) in their measurements. Table 4.3 lists the pressures and optical masses considered as well as the calculated and experimental equivalent widths; the calculations extend from 490.0 to 880.0 cm⁻¹ and the measurements from 495 to 875 cm⁻¹. The optical masses given in the report by Burch et al. (1962) are for S.T.P., we have converted them so that they apply for a temperature of 300°K. The calculations were performed for four pressures, the pressures around 760 mm Hg were run at a pressure of 760 mm Hg, those around 65 mm Hg were run at 65 mm Hg, those around 15 mm Hg at 15.6 mm Hg and the last group at 0.39 mm Hg. The errors introduced by these approximations are small.

We have prepared plots of absorptivity versus frequency and a selected number of these are reproduced in Figure 4.1. We have been very fortunate to have had access to the original spectrophotometer traces of Burch et al. (1962); after suitable normalization some of these have been plotted for comparison in Figure 1. In the case of D 101, D 95, and D83

TABLE 4. 3. Comparison of Calculated and Experimental Equivalent Widths

Identification No. (Burch et al.)	Equivalent Pressure (mm Hg)	Optical Mass (atm cm)	Equivalent Width	
			Calc.	Exp.
D139	755	212. 10	199. 3	183
D133	768	106. 20	178. 6	164
D127	764	51. 00	157. 8	141
D120	762	25. 60	139. 0	125
D80	768	12. 60	120. 4	113
D74	767	6. 30	102. 1	95. 3
D135	65	212. 10	148. 9	143
D89	65	26. 37	95. 9	91. 6
D77	67. 2	12. 64	76. 92	70. 7
D71	63. 6	6. 30	60. 14	54. 7
D46	64. 5	0. 82	24. 46	22. 6
D40	67	0. 42	17. 36	16. 4
D20	63. 5	0. 10	7. 59	7. 11
D22	15. 6	51. 00	80. 71	71. 5
D69	15. 6	6. 30	37. 10	34. 6
D31	15. 9	0. 20	7. 33	7. 46
D156	0. 39	1. 26	4. 84	5. 82
D101	0. 39	0. 64	3. 64	3. 37
D95	0. 39	0. 32	2. 72	2. 66
D83	0. 39	0. 16	2. 04	1. 88

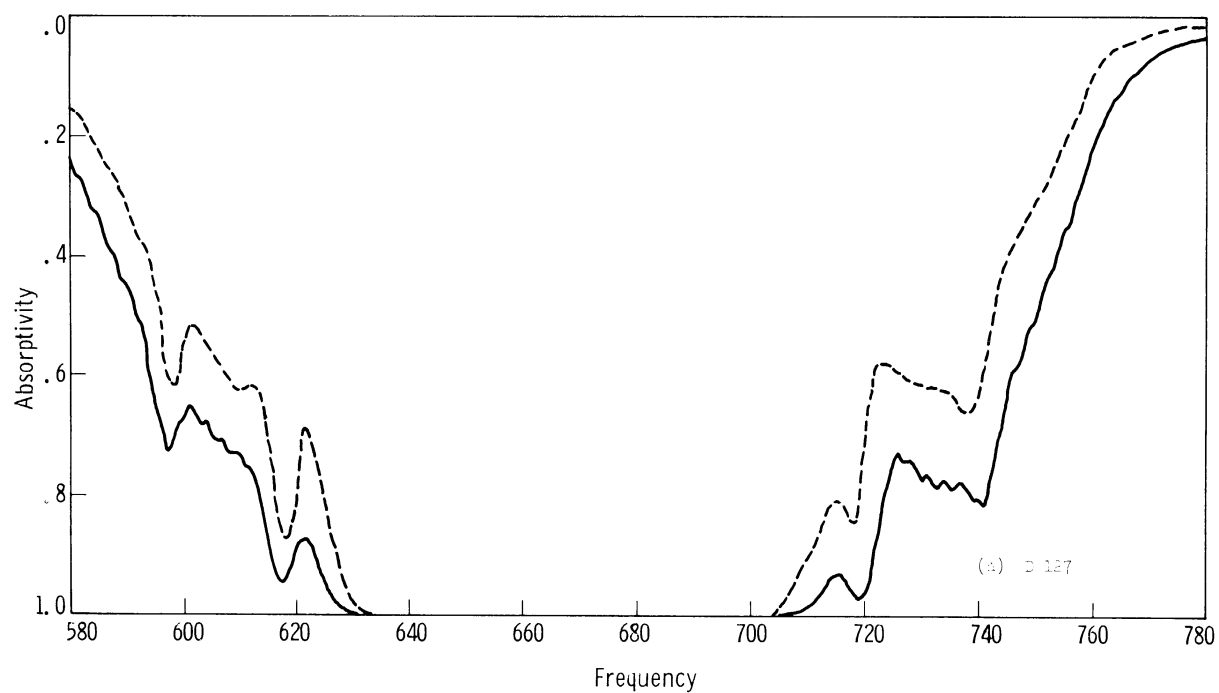


Figure 4.1. Comparison of calculated absorption (solid line) with experimental values of Burch et al. (1962), (dashed line).

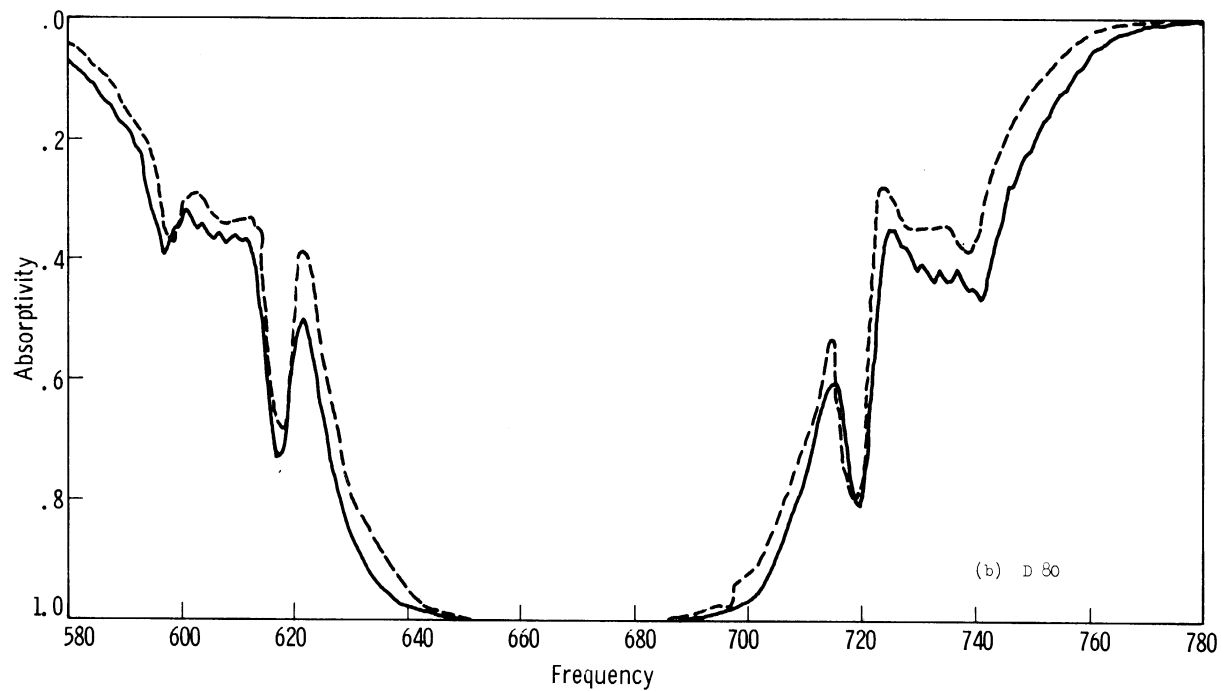


Figure 4.1. Continued.

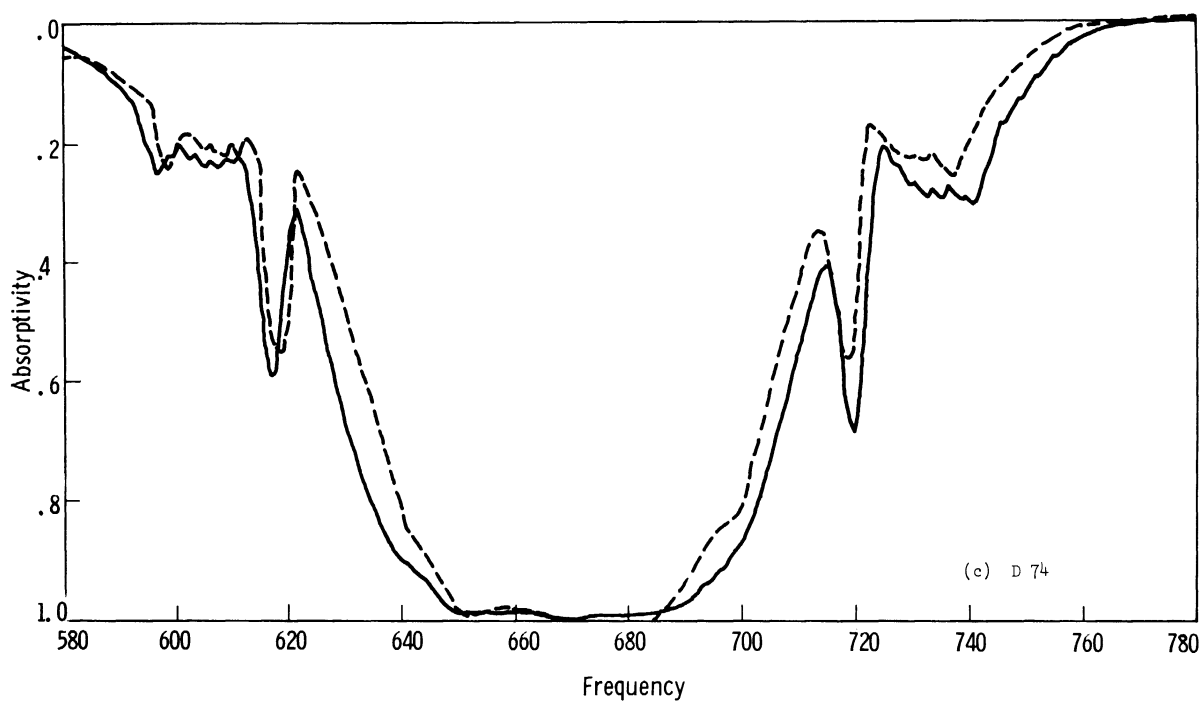


Figure 4.1. Continued.

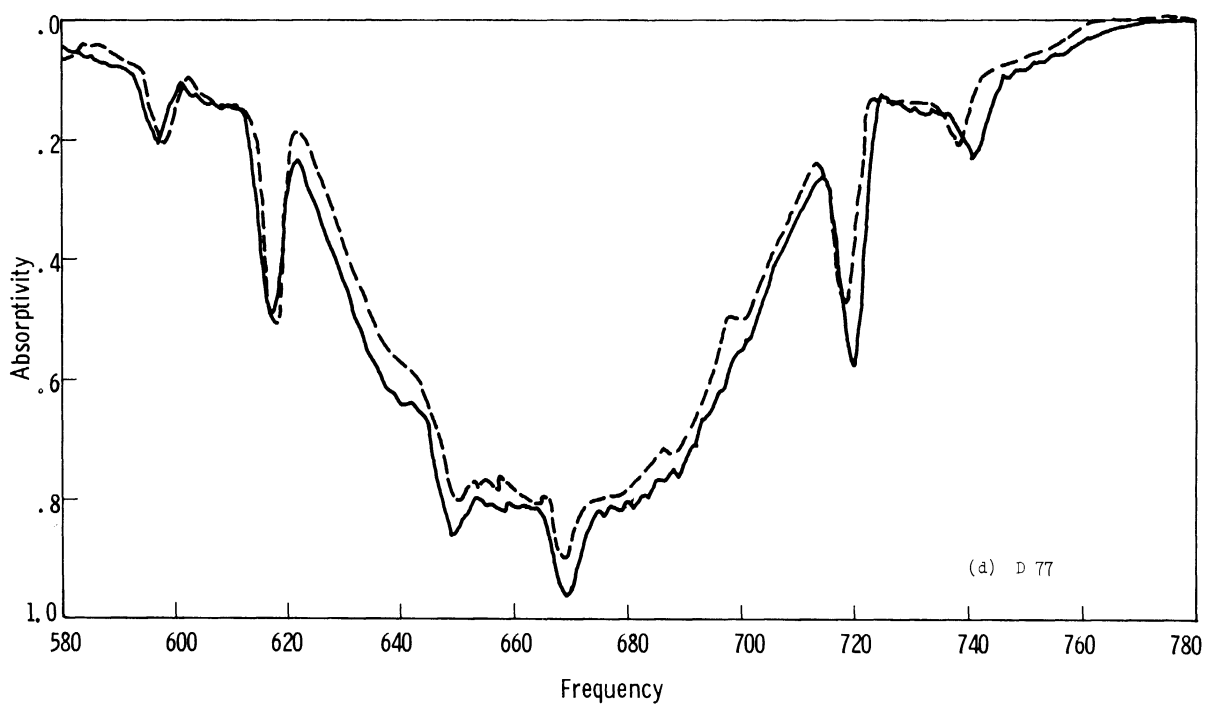


Figure 4.1. Continued.

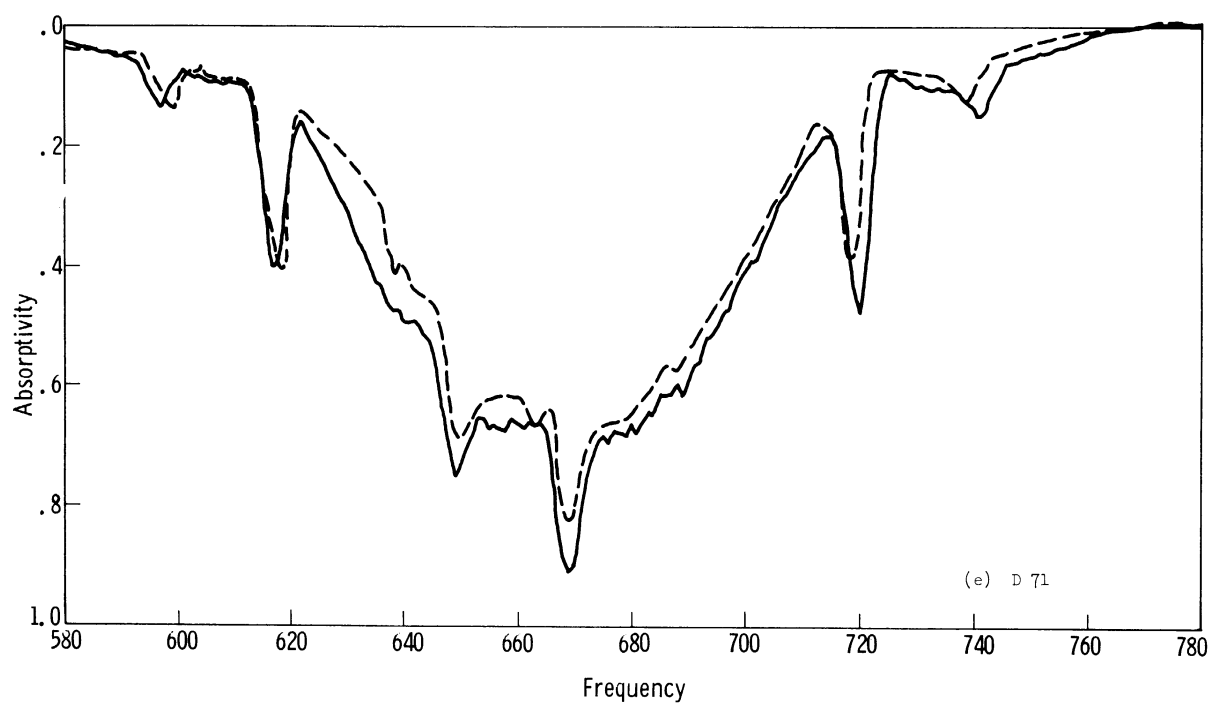


Figure 4.1. Continued.

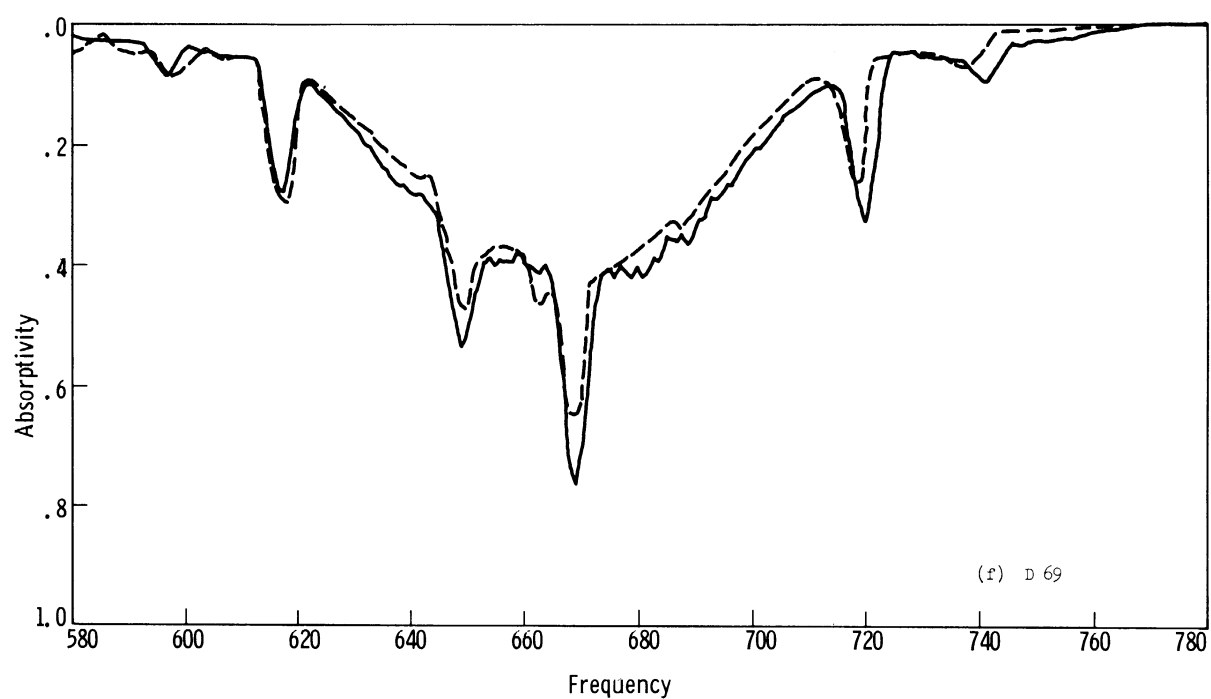


Figure 4.1. Continued.

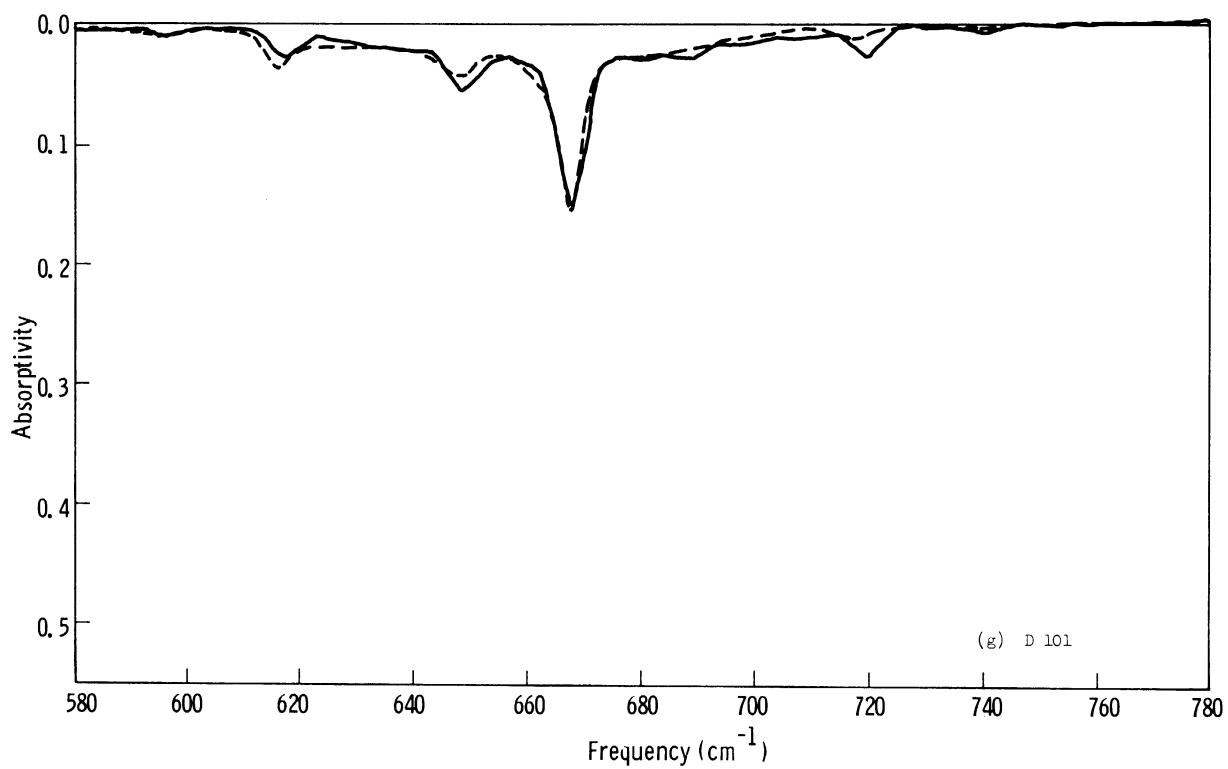


Figure 4.1. Continued.

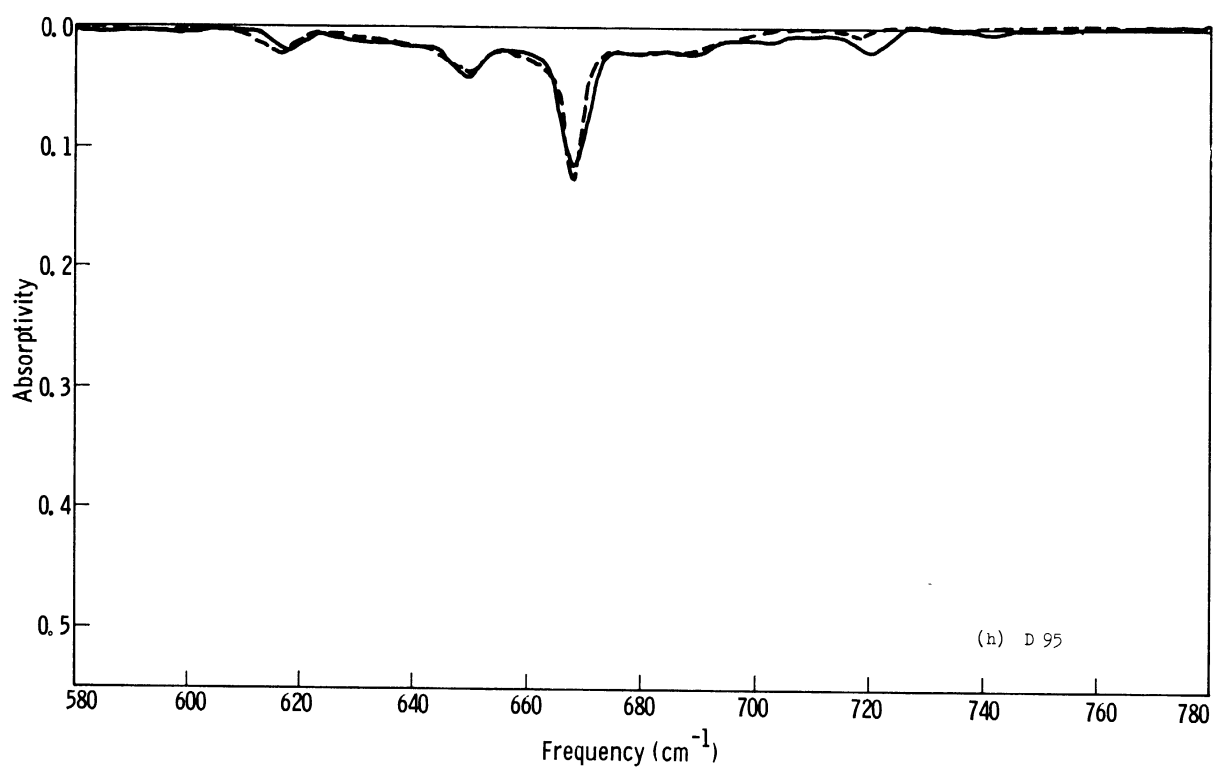


Figure 4.1. Continued.

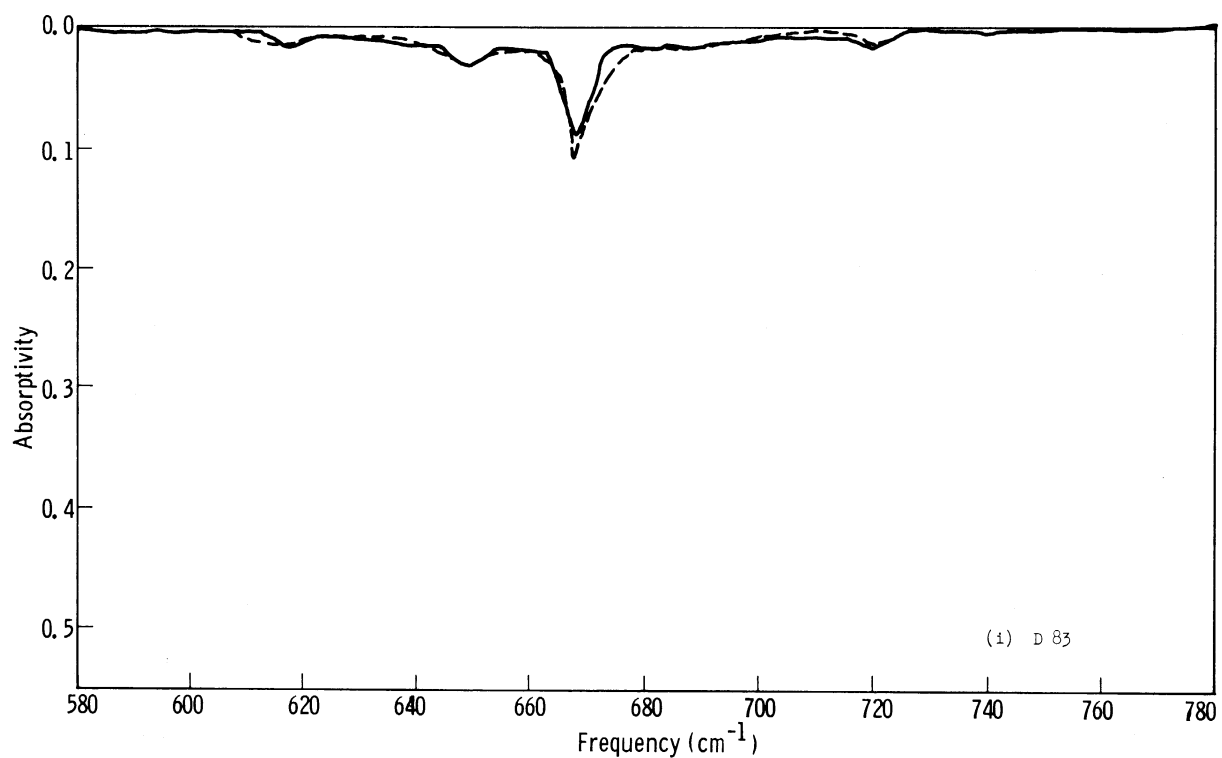


Figure 4.1. Concluded.

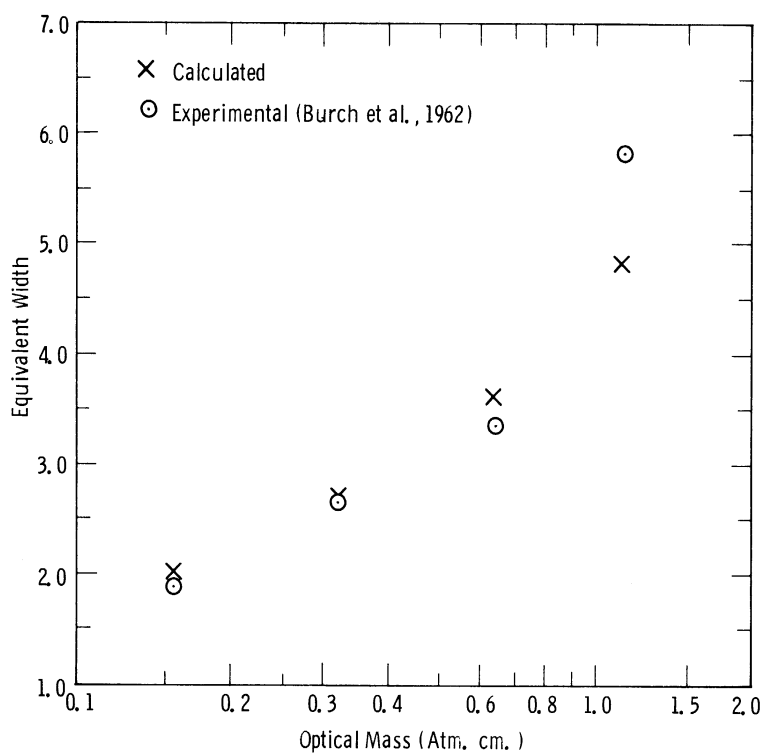


Figure 4.2. Comparison of calculated and experimental absorption at 0.39 mm Hg.

the experimental curves have been taken from the report of Burch et al. (1962). In the plots obtained from the original spectrophotometer traces frequency calibration is not too satisfactory and at the moment we have just centered the calculated and experimental curves with respect to the Q-branch of the ν_2 fundamental. We calculated our absorptivity profile using triangular slit functions with half-widths of 5 cm^{-1} and 4 cm^{-1} . The experimental profiles were taken using programmed slits so that the slit function half-width varied across the spectral region. The calculated curves displayed in Figure 4.1 were obtained using the 4 cm^{-1} half-width; we note that it does not provide quite enough smoothing at the higher frequencies but appears adequate at the lower frequencies.

Examinations of Table 4.3 and Figure 4.1 shows that in our calculations we have overestimated the absorptivity. There is one serious discrepancy in Table 4.3, D 156, where the calculated equivalent width is considerably less than the experimental value. We believe the error is in the experimental equivalent width since if we plot a curve of growth for the four observations D 156, D 101, D 95 and D 83, Figure 4.2, we find that D 156 lies considerably to one side of where we would expect it to lie.

Figure 4.1 shows that we have overestimated the absorptivity for certain bands particularly the ν_2 fundamental. We thus propose in further studies to reduce the intensities of certain bands and recalculate the absorptivity profiles to compare with the experimental profiles. One factor which influences the absorptivity calculations is the Lorentz half-width, but so far we have not studied how changes in this will influence our absorptivity profiles; this is, again, something which we intend to do in the near future.

5. Slant Path Transmissivity

The comparison of the calculations for homogeneous paths with laboratory spectra has shown that the band parameters have to be adjusted to give better agreement between the experimental and theoretical absorption. Despite this limitation, a calculation of slant path absorption was made to compare the theoretically determined radiance with that recorded by the Satellite Infra Red Spectrometer in a balloon flight test, at Palestine, Texas in September, 1964.

First, the transmissivity was computed and averaged over 0.1 cm^{-1} intervals from 660 to 720 cm^{-1} . The program used the Curtis-Godson approximation over the thin layers (see Chapter 3), and computed the transmissivity between the float pressure (10.0 mb) and 23 other pressure levels, using the temperature structure deduced from radiosonde data, Fig. 5.1. A weighting function was applied to the transmissivities to simulate the approximate triangular response function of the SIRS. The results are shown in Tables 5.1 and 5.2. The former is for a fixed resolution of 5 cm^{-1} and the latter for the variable resolution indicated at each frequency. The resolution is unimportant except in the Q-branch at 669.0 cm^{-1} , where the higher resolution gives appreciably more absorption.

Fig. 5.2 is a comparison of the transmissivity calculated above (Table 5.1) with that used by the U. S. Weather Bureau. The greatest difference is in the Q-branch. The two curves are quite similar down to about 25 mb , but below this level the theoretical calculation gives much more absorption. The opposite is true of the channel in the strongest part of the R-branch of the fundamental, at 677.5 cm^{-1} . The Weather Bureau data

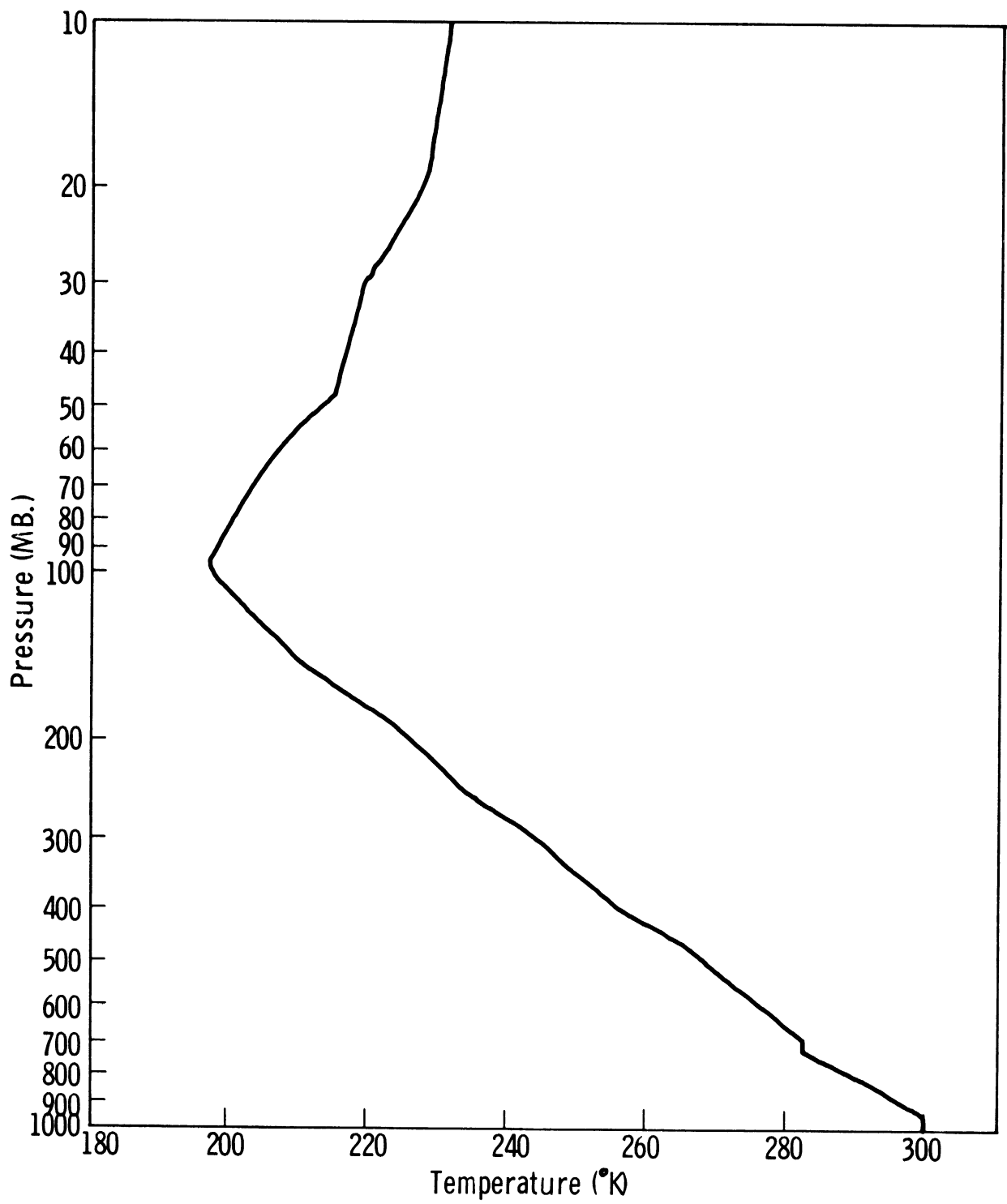


Figure 5.1. Temperature structure for balloon flight.

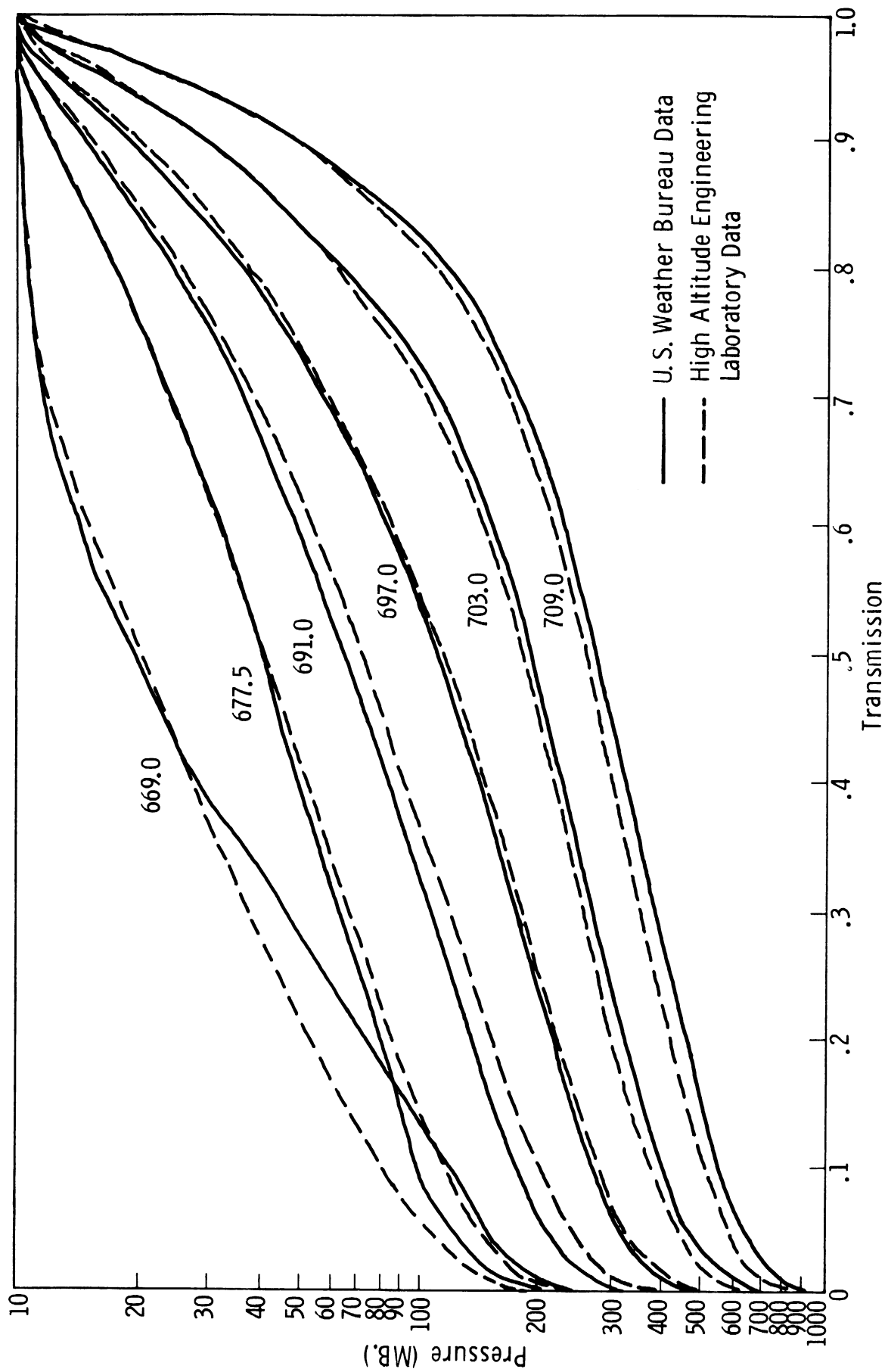


Figure 5.2. Comparison of slant path transmission for U. S. Weather Bureau balloon flight, Palestine, Texas, September, 1964.

TABLE 5.1. Vertical Path Transmissivity from 10.0 mb for SIRS

FREQUENCY	669.0	677.5	691.0	697.0	703.0	709.0	PRESS (MB)	
1.0000	1.0000	1.0000	1.0000	1.0000	1.0000	1.0000	10.00	0
.8396	.9638	.9783	.9864	.9920	.9954	.9954	10.34	1
.7568	.9342	.9603	.9739	.9841	.9903	.9903	11.03	2
.6955	.9035	.9416	.9610	.9760	.9852	.9852	12.07	3
.6547	.8788	.9266	.9508	.9694	.9811	.9811	13.10	4
.5693	.8181	.8895	.9255	.9531	.9708	.9708	16.21	5
.4959	.7561	.8515	.8991	.9362	.9601	.9601	20.00	6
.4228	.6839	.8071	.8679	.9163	.9474	.9474	25.00	7
.3656	.6191	.7667	.8394	.8982	.9360	.9360	30.00	8
.2788	.5065	.6926	.7866	.8647	.9148	.9148	40.00	9
.2151	.4135	.6249	.7375	.8329	.8947	.8947	50.00	10
.1459	.3030	.5347	.6710	.7893	.8673	.8673	65.00	11
.0975	.2190	.4567	.6124	.7504	.8428	.8428	80.00	12
.0547	.1367	.3679	.5431	.7032	.8128	.8128	100.00	13
.0208	.0597	.2560	.4440	.6292	.7641	.7641	130.56	14
.0066	.0210	.1623	.3413	.5392	.7010	.7010	163.64	15
.0017	.0056	.0911	.2417	.4356	.6219	.6219	200.00	16
.0002	.0007	.0364	.1378	.3042	.5077	.5077	250.00	17
.0000	.0000	.0120	.0689	.1942	.3922	.3922	302.50	18
.0000	.0000	.0011	.0145	.0710	.2165	.2165	400.00	19
.0000	.0000	.0001	.0019	.0198	.0994	.0994	500.00	20
.0000	.0000	.0000	.0000	.0013	.0178	.0178	660.00	21
.0000	.0000	.0000	.0000	.0001	.0033	.0033	800.00	22
.0000	.0000	.0000	.0000	.0000	.0003	.0003	1000.00	23
RESOLUTION	5.0	5.0	5.0	5.0	5.0	5.0		

TABLE 5.2. Vertical Path Transmissivity from 10.0 mb for SIRS

FREQUENCY	669.0	677.5	691.0	697.0	703.0	709.0	PRESS (MB)	
1.0000	1.0000	1.0000	1.0000	1.0000	1.0000	1.0000	10.00	0
.8310	.9639	.9783	.9864	.9920	.9954	.9954	10.34	1
.7441	.9344	.9603	.9738	.9841	.9903	.9903	11.03	2
.6801	.9037	.9416	.9609	.9759	.9852	.9852	12.07	3
.6378	.8791	.9266	.9507	.9694	.9811	.9811	13.10	4
.5500	.8184	.8895	.9254	.9531	.9708	.9708	16.21	5
.4752	.7565	.8515	.8989	.9361	.9600	.9600	20.00	6
.4016	.6843	.8071	.8677	.9162	.9473	.9473	25.00	7
.3446	.6195	.7667	.8391	.8982	.9359	.9359	30.00	8
.2596	.5068	.6926	.7864	.8646	.9146	.9146	40.00	9
.1984	.4137	.6249	.7372	.8328	.8945	.8945	50.00	10
.1330	.3031	.5347	.6707	.7892	.8670	.8670	65.00	11
.0878	.2191	.4567	.6122	.7503	.8425	.8425	80.00	12
.0487	.1367	.3679	.5429	.7030	.8124	.8124	100.00	13
.0181	.0597	.2560	.4438	.6290	.7636	.7636	130.56	14
.0056	.0210	.1623	.3412	.5391	.7004	.7004	163.64	15
.0014	.0056	.0911	.2416	.4358	.6213	.6213	200.00	16
.0002	.0007	.0364	.1378	.3047	.5072	.5072	250.00	17
.0000	.0000	.0120	.0689	.1949	.3919	.3919	302.50	18
.0000	.0000	.0011	.0145	.0718	.2167	.2167	400.00	19
.0000	.0000	.0001	.0019	.0203	.1000	.1000	500.00	20
.0000	.0000	.0000	.0000	.0014	.0184	.0184	660.00	21
.0000	.0000	.0000	.0000	.0001	.0035	.0035	800.00	22
.0000	.0000	.0000	.0000	.0000	.0003	.0003	1000.00	23
RESOLUTION	4.6	4.8	5.0	5.1	5.2	5.3		

indicates rather more absorption below the 50 mb level. It should be noted that the present calculations do not give a cross-over of the absorption curves for these two channels.

The four channels from 691.0 to 709.0 cm^{-1} form a family with similar characteristics. The curves from the two sources are very similar in shape, only slightly displaced from each other. The present calculations give less absorption at 691.0 cm^{-1} , almost the same at 697.0 cm^{-1} , and rather more absorption at 703.0 and 709.0 cm^{-1} .

The transmissivity values have been used to calculate the vertical component of radiance at the balloon level, and are shown together with the observed value in Table 5.3. The Q-branch channel at 669.0 cm^{-1} did not perform properly during the instrument flight, so the measured value should be ignored. The present calculations show good agreement at 677.5, 691.0 and 697.0 cm^{-1} , but considerable divergence at 703.0 and 709.0 cm^{-1} . This result was anticipated, since the higher frequencies are quite sensitive to errors in estimation of the absorption, whereas the lower ones are comparatively insensitive. The present calculations are known to overestimate the absorption and hence underestimate the radiance for the four channels from 691.0 to 709.0 cm^{-1} . When more realistic values of the band parameters become available, it is expected that the calculated radiance will come quite close to the observed values, at least to within the experimental error.

It has been shown that the present calculations overestimate the absorption for all of the six channels. For some of the channels this makes

little difference to the computed radiances, for the temperature profile used. If other profiles are used, however, the differences may become much greater, so that it becomes a matter of importance to obtain more accurate values for all the channels.

Table 5.3. Vertical components of radiance at 10 mb
for U. S. Weather Bureau Texas balloon flight

Frequency (cm^{-1})	Radiance ($\text{ergs cm}^{-2} \text{sec.}^{-1} \text{strdn.}^{-1}/\text{cm}^{-1}$)		
	Measured	Present Calculation	Calculated from U. S. Weather Bureau Data
669.0	(49.6)	48.0	47.3
667.5	42.4	41.6	41.5
691.0	40.1	40.2	39.3
697.0	43.6	43.5	42.9
703.0	52.2	50.2	52.3
709.0	64.9	60.6	64.0

6. Conclusions

The main conclusion that we can draw from the previous discussion is that we must re-estimate our band intensities and it is evident that most of them are too strong. The value of Lorentz half-width (0.08 cm^{-1} at 1 atm. and 300°K) that we used, while appearing to give satisfactory results, should be varied in subsequent calculations so that its influence on the transmissivity calculations can be comprehensively studied. One important consideration that became evident during our work was that it is very important to obtain good agreement between calculated and experimental absorptivity profiles for many pressures and optical masses and not just a selected few.

One factor which has caused us some trouble in our calculations has been the sparsity of experimental measurements to check with our calculations. We obviously need more low and high resolution measurements, the low and high resolution measurements complementing each other.

Finally, we have not studied the influence of the 14-micron ozone band and the rotational water vapor lines on atmospheric transmissivities in the 15-micron region. No reliable estimates of their influence are available and we suggest that this area might be profitably studied.

Acknowledgments

The authors are grateful for the constant help and encouragement given by F. L. Bartman, Project Supervisor and L. M. Jones, Project Director. D. L. Childs and W. Lee provided invaluable assistance during the preparation of the programs. We are very grateful for the information we received during our conversations with the staff of the Meteorological Satellite Laboratory, in particular Dr. D. Q. Wark. Dr. John Shaw of Ohio State University gave freely of his time and let us use some of the original spectrophotometer tracings for carbon dioxide transmissivities which were taken in his laboratory. We also received valuable advice from Dr. W. S. Benedict of The Johns Hopkins University.

This work is a continuation of research originally sponsored by NASA under Contract No. NASr-54(03) and by NSF under Grant No. G-19131.

References

- Allen, H. C., Jr. and P. C. Cross, 1963: Molecular vib-rotors. Wiley and Sons, Inc., New York.
- Amat, G., and M. Pimbert, 1965: On Fermi resonance in carbon dioxide. J. Mol. Spect., 16, 278-290.
- Benedict, W. S., 1957: Comments on the spectra of telluric H₂O and CO₂ as observed in the solar spectrum, 2.8-23.7 μ , in the solar spectrum from 2.8 to 23.7 microns Part II. Mem. Soc. Roy. Sci., Lièges. Special Vol. No. 2.
- Burch, D. E., E. B. Singleton and D. Williams, 1962: Absorption line broadening in the infrared. App. Optics, 1, 359-363.
- Burch, D. E., D. Gryvnak and D. Williams, 1962: Absorption by carbon dioxide. Part B of, Infrared absorption by carbon dioxide, water vapor and minor atmospheric constituents. AFCRL-62-698.
- Burch, D. E., D. A. Gryvnak and R. R. Patty, 1965: Absorption by CO₂ between 8000 and 10000 cm⁻¹. Publication No. U-3200, Aeronutronic Division of Philco Corp., Newport Beach, California.
- Courtoy, C.-P., 1959: Spectre infrarouge a grande dispersion et constantes moléculaires du CO₂. Ann. Soc. Sci. Bruxelles, 73, 5-230.
- Dennison, D. M., 1931: The infrared spectra of poly atomic molecules. Rev. Mod. Phys., 3, 280-345.
- Drayson, S. R., 1964: Atmospheric slant path transmission in the 15 μ CO₂ band. Univ. of Michigan Technical Report 05863-6-T. Reprinted as NASA Technical Note TN-D 2744.
- Drayson, S. R., 1966: Atmospheric transmission in the CO₂ bands between 12 and 18 μ . App. Optics, 5, 385-391.
- Gates, D. M., and R. F. Calfee, 1963: Computed transmission spectra for 2.7-micron H₂O band. App. Optics, 2, 1117-1122.
- Gates, D. M., and R. F. Calfee, 1966: Calculated slant-path absorption and distribution of atmospheric water vapor. App. Optics, 5, 287-292.
- Goody, R. M., 1964: Atmospheric radiation I: Theoretical basis. Oxford University Press, Oxford.
- Gordon, H. R., and T. K. McCubbin, Jr., 1965: The 15-micron bands of C¹² O₂¹⁶. J. Mol. Spect., 18, 73-82.

- Gordon, H. R., and T. K. McCubbin, Jr., 1966: The 2.8-micron bands of CO₂. J. Mol. Spect., 19, 137-154.
- Gray, S. D., and R. A. McClatchey, 1965: Calculations of atmospheric radiation from 4.2 μ to 5 μ . App. Optics, 4, 1624-1631.
- Gray, L. D., and J. E. Selvidge, 1965: Relative intensity calculations for carbon dioxide, Part I. Internal partition function. J. Quant. Spectrosc. Rad. Trans., 5, 291-295.
- Herzberg, G., 1945: Infrared and Raman spectra of polyatomic molecules. van Nostrand Co., Inc. Princeton, New Jersey.
- Hitschfeld, W., and J. T. Houghton, 1961: Radiative transfer in the lower stratosphere due to the 9.6 micron band of ozone. Quart. J. Roy. Met. Soc., 87, 562-577.
- Kaplan, L. D., and D. F. Eggers, 1956: Intensity and line-width of the 15-micron CO₂ band determined by a curve-of-growth method. J. Chem. Phys., 25, 876-883.
- Madden, R. P., 1961: A high resolution study of CO₂ absorption spectra between 15- and 18-microns. J. Chem. Phys. 35, 2083-2097.
- National Environmental Satellite Lab. E.S.S.A., 1966: Private communication.
- Overend, J., M. J. Youngquist, E. C. Curtis, and B. Crawford, 1959: Vibrational intensities XI. CO₂ and the Wilson-Wells method. J. Chem. Phys. 30, 532-537.
- Penner, S. S., 1959: Quantitative Molecular spectroscopy and gas emissivities. Addison-Wesley, Reading.
- Plass, G. N., 1958: Models for spectral band absorption. J. Opt. Soc. Am., 48, 690-703.
- Schurin, D., 1960: Calculated band intensities for CO₂ from infrared dispersion data. J. Chem. Phys., 33, 1878.
- Shaw, J. H., and J. T. Houghton, 1964: Total band absorptance of CO near 4.7 μ . App. Optics 3, 773-779.
- Stull, V. R., P. J. Wyatt and G. N. Plass, 1962: Vibrational energies of the CO₂ molecule. J. Chem. Phys., 37, 1442-1445.
- Thorndike, A. M., 1947: The experimental determination of the intensities of infrared absorption bands, III. Carbon dioxide, methane and ethane. J. Chem. Phys., 15, 868-874.

- Varanasi, P., and J. L. Lauer, 1966: Determination of the integrated intensity of the 15-micron bands of carbon dioxide. J. Quant. Spect. Rad. Trans., 6, 127-130.
- Weber, D., R. J. Holm and S. S. Penner, 1952: Integrated absorption for vibration-rotational bands of CO₂. J. Chem. Phys., 20, 1820.
- Winters, B. H., S. Silverman and W. S. Benedict, 1964: J. Quant. Spect. Rad. Trans., 4, 527-537.
- Yamamoto, G., and T. Sasamori, 1958: Calculations of the absorption of the 15-micron carbon dioxide band. Science Reports, Tohoku Univ., 5th Series (Geophysics), 10, 37-57.
- Yamamoto, G., and T. Sasamori, 1964: Analysis of the 15-micron CO₂ absorption measurements. Geophysical Institute, Tohoku Univ. Contract Cwb-10548, U. S. W. B.
- Young, C., 1965: Calculation of the absorption coefficient for lines with combined Doppler and Lorentz broadening. J. Quant. Spect. Rad. Trans., 5 549-552.

UNIVERSITY OF MICHIGAN



3 9015 02844 0231